

# Influence of zinc addition on the precipitation in Al-Mn-Zr alloys

M. Karlík<sup>1,2\*</sup>, M. Vronka<sup>1</sup>, P. Haušild<sup>1</sup>, O. Kovářik<sup>1</sup>

<sup>1</sup>Czech Technical University in Prague, Faculty of Nuclear Sciences and Physical Engineering, Department of Materials, Trojanova 13, 120 00 Prague 2, Czech Republic

<sup>2</sup>Department of Physics of Materials, Charles University, Ke Karlovu 5, 121 16 Prague 2, Czech Republic

Received 14 July 2017, received in revised form 17 October 2017, accepted 31 October 2017

## Abstract

Two Al-Mn-Zr alloys produced by twin-roll casting having almost the same chemical composition except for the content of zinc (0.10 and 1.66 wt.%, respectively) were investigated. Precipitation reactions during two-step annealing were examined by means of electrical conductivity and differential scanning calorimetry. Furthermore, SEM quantitative particle analysis, energy dispersive spectroscopy, and electron backscattered diffraction were carried out. The results show that 1.1 to 1.8 wt.% of zinc enters into constituent  $\text{Al}_{15}(\text{Mn,Fe})_3\text{Si}_2$  phases and that zinc improves nucleation of small Al(Mn,Fe)Si particles, 20 to 100 nm in size, which is beneficial for the recrystallization resistance of the alloy.

**Key words:** Al-Mn-Zr alloys, Zn addition, microstructure, SEM quantitative particle analysis, phase analysis

## 1. Introduction

Al-Mn-Zr alloys, having high specific strength, thermal conductivity, good formability, and corrosion resistance, are frequently used in heat exchangers for automobiles. The majority of these heat exchangers are manufactured using controlled atmosphere brazing process, during which an assembly of tubes and fins, tied strongly by steel wires, is exposed to a temperature increase up to 600°C. Hence, the material should be very resistant to recrystallization to keep its strength and to avoid the collapse of the structure [1]. High recrystallization resistance can be attained by a dense and homogeneous distribution of second phase particles to strengthen the matrix and also to provide anchor points on subgrain and grain boundaries (Zener drag) [2]. In Al-Mn-Zr alloys, there are two types of dispersoids, Mn-bearing and Zr-bearing. The equilibrium phase in Al-Mn system is  $\text{Al}_6\text{Mn}$ . Nevertheless, when the iron is present, it substitutes for manganese giving  $\text{Al}_6(\text{Mn,Fe})$  [3, 4]. Silicon is a frequent impurity in aluminium, and so Al(Mn,Fe)Si phases are formed as well [5]. In the alloys containing more Si than Fe only hexagonal and cubic  $\alpha$ -Al(Mn,Fe)Si phases with composition  $\text{Al}_{12}(\text{Mn,Fe})_3\text{Si}$

or  $\text{Al}_{15}(\text{Mn,Fe})_3\text{Si}_2$  were observed [6, 7]. Nonetheless, for a very high recrystallization resistance, a fine dispersion of the Mn-bearing particles is often insufficient, and other additives are necessary. The highest anti-recrystallization effect could be achieved by alloying with scandium, which forms  $\text{Al}_3\text{Sc}$  dispersoids [8]. However, Sc is very expensive to be used in automotive industry, where the lowest possible prices are required. Therefore, zirconium addition, leading to the formation of small coherent particles of  $\text{Al}_3\text{Zr}$ , has been proposed [9, 10]. Zirconium is usually heterogeneously distributed in the aluminium matrix due to the segregation during solidification and its low diffusivity. An attempt to minimize Zr segregation by homogenizing an Al-Mn-Zr alloy at 630°C did not improve the distribution and the number density of  $\text{Al}_3\text{Zr}$  particles [10]. A denser and more homogeneous dispersion of  $\text{Al}_3\text{Zr}$  dispersoids was achieved by pre-annealing at 250°C before final precipitation annealing at 450°C with slow heating rate [11]. The addition of zinc, which is distributed mainly in the solid solution in the aluminium matrix, in concentrations up to 2 wt.%, leads to a modest improvement of mechanical properties [12]. On the other hand, the change of the corrosion potential of the alloy is important [13]. Ac-

\*Corresponding author: tel.: +420 224 358 507; fax: +420 224 358 523; e-mail address: [Miroslav.Karlik@fjfi.cvut.cz](mailto:Miroslav.Karlik@fjfi.cvut.cz)

Table 1. Chemical composition of alloys (wt.%)

Alloy	Mn	Zn	Fe	Si	Cu	Zr	Al
A	1.05	0.10	0.18	0.49	0.13	0.17	Balance
B(Zn)	1.03	1.66	0.23	0.55	0.15	0.15	Balance

cordingly, fins from the Al-Mn-Zr alloys with Zn are utilized as sacrificial materials to protect the tubes in the exchangers from corrosion [14].

This paper aims to report the influence of the zinc addition on the precipitation of  $\alpha$ -Al(Mn,Fe)Si and Al<sub>3</sub>Zr dispersoids during two-step precipitation annealing of an Al-Mn-Zr alloy prepared by twin-roll casting in the industrial conditions.

## 2. Experimental details

Two Al-Mn-Zr alloys with different Zn addition (0.10 and 1.66 wt.%, respectively, see Table 1 for more details) were produced by twin-roll casting in industrial conditions and further processed in the laboratory. The cast strips, 8.5 mm in thickness, were cold rolled with thickness reduction of 39 % (equivalent strain  $\varepsilon \sim 0.57$ ), and then subjected to a two-step precipitation annealing which consisted of 15 h heating to 250 °C (0.27 K min<sup>-1</sup>), soaking for 12 h, 13 h heating to 450 °C (0.25 K min<sup>-1</sup>), and soaking for 10 h at this temperature followed by cooling down 1.5 K min<sup>-1</sup>. The scheme of annealing procedure is given as a background plot in the graph of the evolution of electrical conductivity (Fig. 4a). Samples were taken at different stages of annealing. The precipitation reactions during annealing and the changes in solid solution concentration were monitored by differential scanning calorimetry in a Netzch Pegasus 40C apparatus with a heating rate of 20 °C s<sup>-1</sup> and also by using eddy current electrical conductivity probe (Foerster Sigmatest device). The grain structure was observed by light metallographic microscope Nikon Epiphot 300 equipped with the camera Hitachi-HBC 20A, in polarized light after electrolytic anodic oxidation ( $J = 0.2 \text{ A cm}^{-2}$  for 40–80 s, room temperature) in Barker's reagent (5 ml HBF<sub>4</sub> (48 %) + 200 ml H<sub>2</sub>O). The second phase particles were revealed by etching with a 0.5 % solution of hydrofluoric acid in water. Coarser particles in the precipitation annealed samples were analysed by energy dispersive X-ray spectroscopy (EDXS) in the scanning electron microscope (SEM) FEI Quanta 200F equipped with a Schottky type field-emission gun (FEG) operating at 20 kV and also by electron back-scattering diffraction (EBSD) phase analysis according to their crystallographic structure. Besides this general microstructure examination, a quantitative second phase particle analysis on the series of

FEG-SEM micrographs was carried out. The microscope was operated at 5 kV in the backscattered electron (BSE) signal. From each sample, 20 micrographs at the magnification 5000 $\times$ , and 20 micrographs at the magnification 50 000 $\times$  were recorded to examine coarse and fine second phase particles, respectively. This number of micrographs enabled to analyse more than 3000 particles to have a statistically sufficient dataset [15]. The sets of micrographs were first normalized to have a constant mean value and standard deviation of brightness and then automatically processed by the software written in Matlab [16], using toolboxes Image Processing and Statistics.

## 3. Results and discussion

In both materials, light microscopy revealed similar microstructure typical for twin-roll casting. The grains, flattened to some extent after cold rolling, are oriented diagonally from the rolls to the centre of the strip (Fig. 1a,d); their lateral dimension is about 70  $\mu\text{m}$  and length around 500  $\mu\text{m}$ . The alloy A has a somewhat wider band of the centerline segregation (Figs. 1b,c) than the alloy B(Zn) (Figs. 1e,f). The distribution of coarse intermetallic phases shows only negligible differences, besides the centerline segregation, there are elongated colonies of fine particles in both alloys (Figs. 1c,f).

The crystal structure of these coarse constituent particles has been studied using EBSD; their chemical composition was determined using EDXS point analysis [17, 18]. The resulting data of the content of Mn + Fe vs Si are plotted in Fig. 2. From the graph, it is obvious that nearly all of the particles are of the  $\alpha$ -Al<sub>15</sub>(Mn,Fe)<sub>3</sub>Si<sub>2</sub> phase. From 20 particles analysed in both alloys, only two in alloy A had Mn+Fe/Si ratio corresponding to the  $\alpha$ -Al<sub>12</sub>(Mn,Fe)<sub>2</sub>Si phase. From the EDXS measurements, it also follows that zinc enters into Al(Mn,Fe)Si constituent phases. This is in agreement with results of Jaradeh and Carlberg [13]. All examined particles in alloy B(Zn) contained 1.1 to 1.8 wt.% of zinc, these values being very close to the Zn concentration in the matrix (1.66 wt.% Zn). The EBSD crystal structure analysis has shown that the majority of particles are of the cubic  $\alpha$ -Al<sub>15</sub>(Mn,Fe)<sub>3</sub>Si<sub>2</sub> phase (*Im-3*, space group 204,  $a = 1.25 \text{ nm}$ ). The results for the alloy A (not shown here) yielded 80 % of cubic, and 20 % of hexagonal

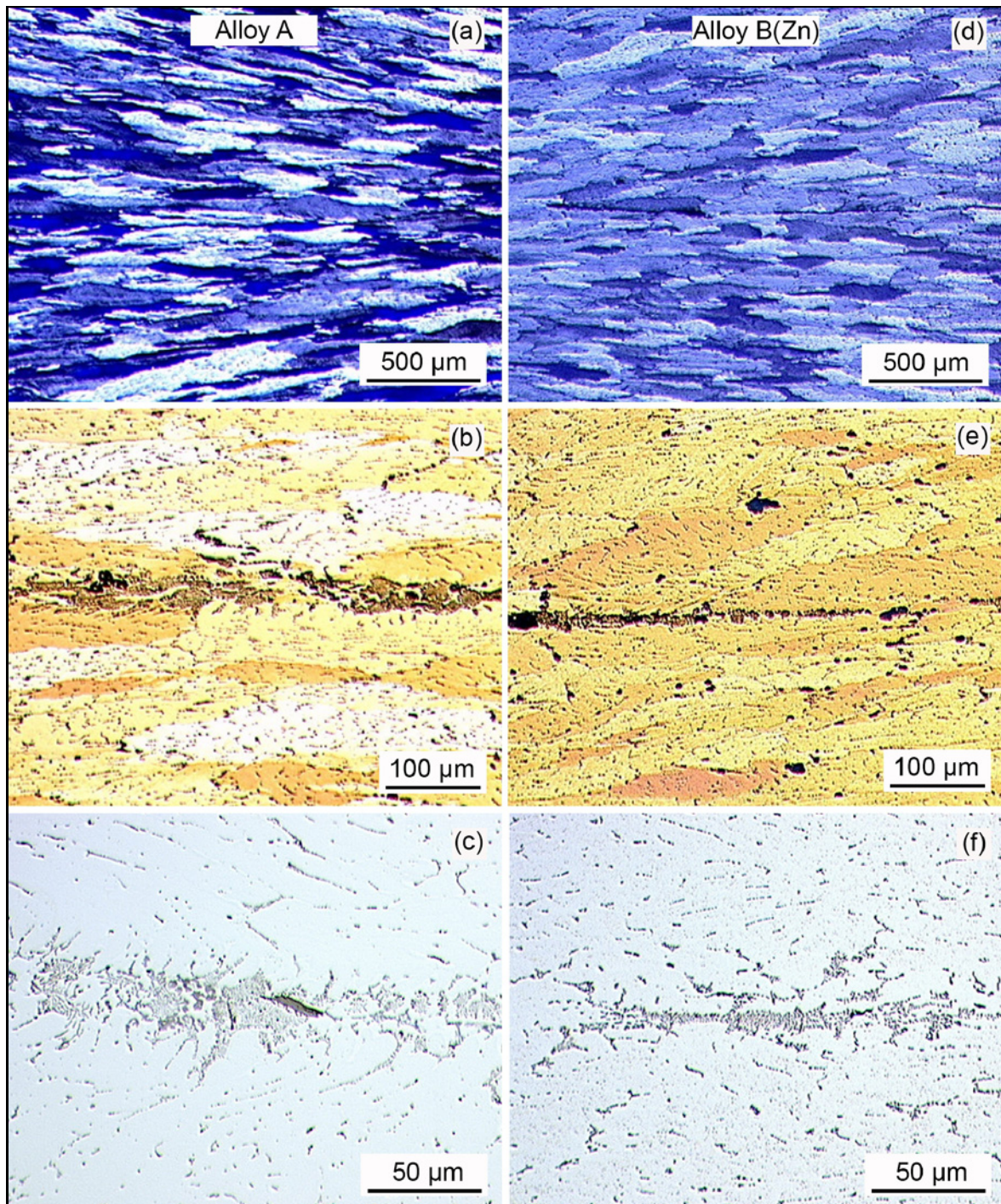


Fig. 1. Light micrographs of alloys in the as-received condition, after twin-roll casting and cold rolling with reduction of 39 %. Grain structure in polarized light after anodizing with Barker's reagent (Figs. 1a–e). Particles revealed by etching in 0.5 % solution of HF in water (Figs. 1c,f).

$\alpha$ -Al<sub>15</sub>(Mn,Fe)<sub>3</sub>Si<sub>2</sub> phase (*Pm-3m*, space group 221,  $a = 1.24$  nm,  $c = 2.62$  nm) [19]; the corresponding EBSD scan of the alloy B(Zn) (Fig. 3) exhibits 94 % of cubic  $\alpha$ -phase and 6 % of hexagonal  $\alpha$ -phase.

The effect of two-step precipitation annealing was examined by electrical conductivity and differential scanning calorimetry. Figure 4a presents the evolution

of electrical conductivity with annealing time; for the sake of clarity, the corresponding temperature course is also plotted. It can be seen that there are three dissimilar stages. In the first stage, corresponding to heating to 250 °C and soaking at this temperature, the conductivity slightly increases due to clustering of solute elements [20]. During the next stage, associated

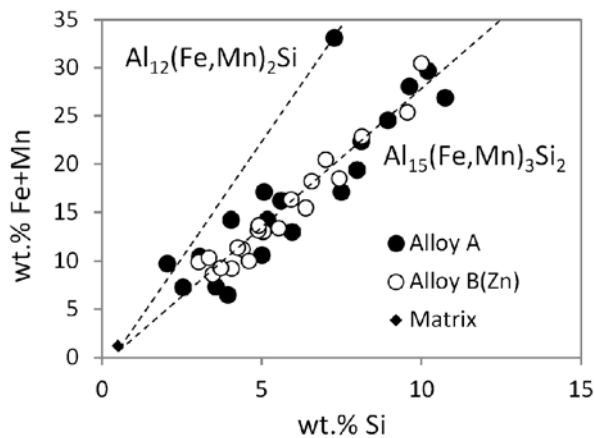


Fig. 2. Composition map Fe + Mn vs Si of coarse constituent intermetallic particles from EDXS point analysis.

with heating to 450°C, an important increase of the electrical conductivity appears due to the transfer of the solute atoms from the aluminium matrix to second phase particles. In the third stage of annealing, related to soaking at 450°C and cooling down to room temperature, the electrical conductivity exhibits again a slow increase due to nucleation of new dispersoids of  $\alpha$ -Al(Mn,Fe)Si phase from the remaining solutes in the matrix (observed up to 500°C [21]) and coarsening of particles. In this third stage, the alloy B(Zn) shows lower values of electrical conductivity due to a

higher concentration of Zn in the solid solution. Unlike the electrical conductivity measurements on separate samples after different periods of annealing, the differential scanning calorimetry (DSC) enables a continuous *in situ* insight into the precipitation process. The DSC plot corresponding to heating at the rate of 20°C min<sup>-1</sup> from 150 to 535°C is shown in Fig. 4b. At both curves, there are two distinct exothermic peaks, corresponding to the precipitation of dispersoids of  $\alpha$ -Al(Mn,Fe)Si phase. The influence of the formation of Al<sub>3</sub>Zr could be excluded, due to the very slow kinetics of the nucleation and growth of these particles and the fact that the alloy has been cold rolled [22]. According to Cieslar et al. [7], the first peak, approximately at 365°C, marked I, corresponds to the precipitation of  $\alpha$ -Al(Mn,Fe)Si phase at subgrain and grain boundaries, and the second one, at about 480°C, marked II, to the precipitation of the same phase in the matrix [7]. From the comparison of the DSC curves, it is obvious that the peak I of B(Zn) alloy is more pronounced, indicating precipitation of a higher number density of fine  $\alpha$ -Al(Mn,Fe)Si dispersoids 20 to 100 nm in size (Figs. 5c, 6a). The peak II is, on the contrary, more pronounced in the case of the alloy A and it is somewhat shifted to lower temperature, since the solutes in the aluminium matrix which did not contribute to the formation of particles in the temperature range from 300 to 420°C (peak I) enhanced and accelerated the precipitation in the temperature range from 445 to 500°C (peak II).

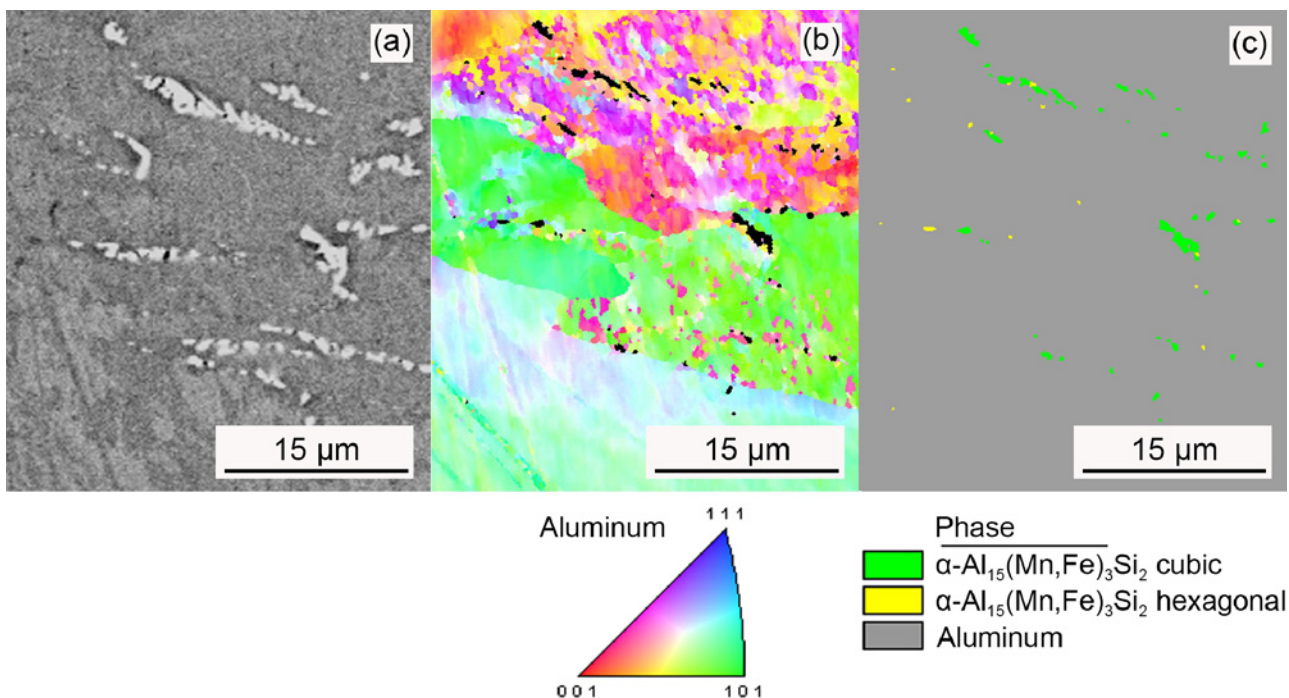


Fig. 3. EBSD analysis of the B(Zn) alloy: (a) backscattered electron micrograph, (b) orientation map, (c) identification of the particles according to crystallographic data.

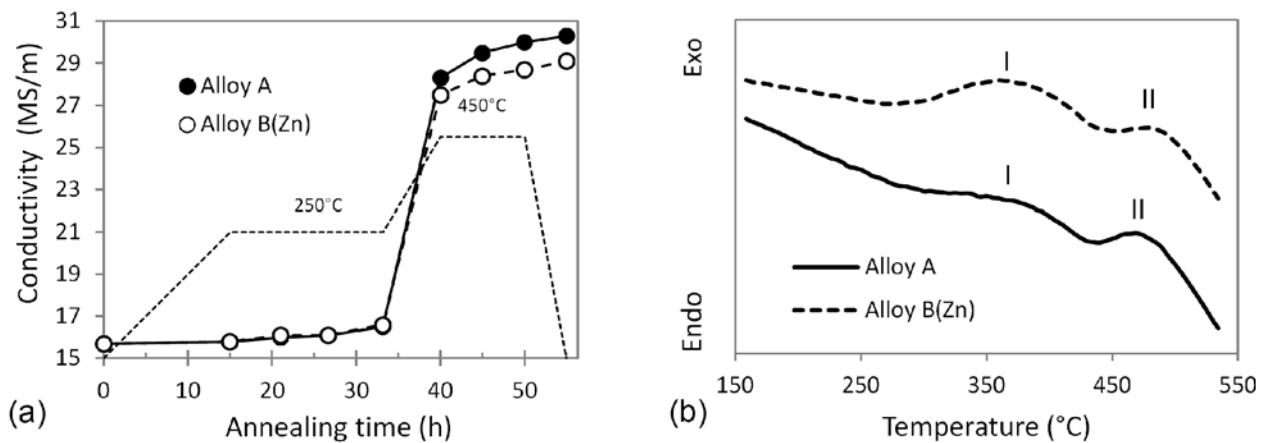


Fig. 4. (a) The evolution of electrical conductivity during two-step precipitation annealing; for the sake of clarity, the corresponding temperature course is also plotted; (b) DSC curves during heating  $20^{\circ}\text{C min}^{-1}$  from 150 to  $540^{\circ}\text{C}$ .

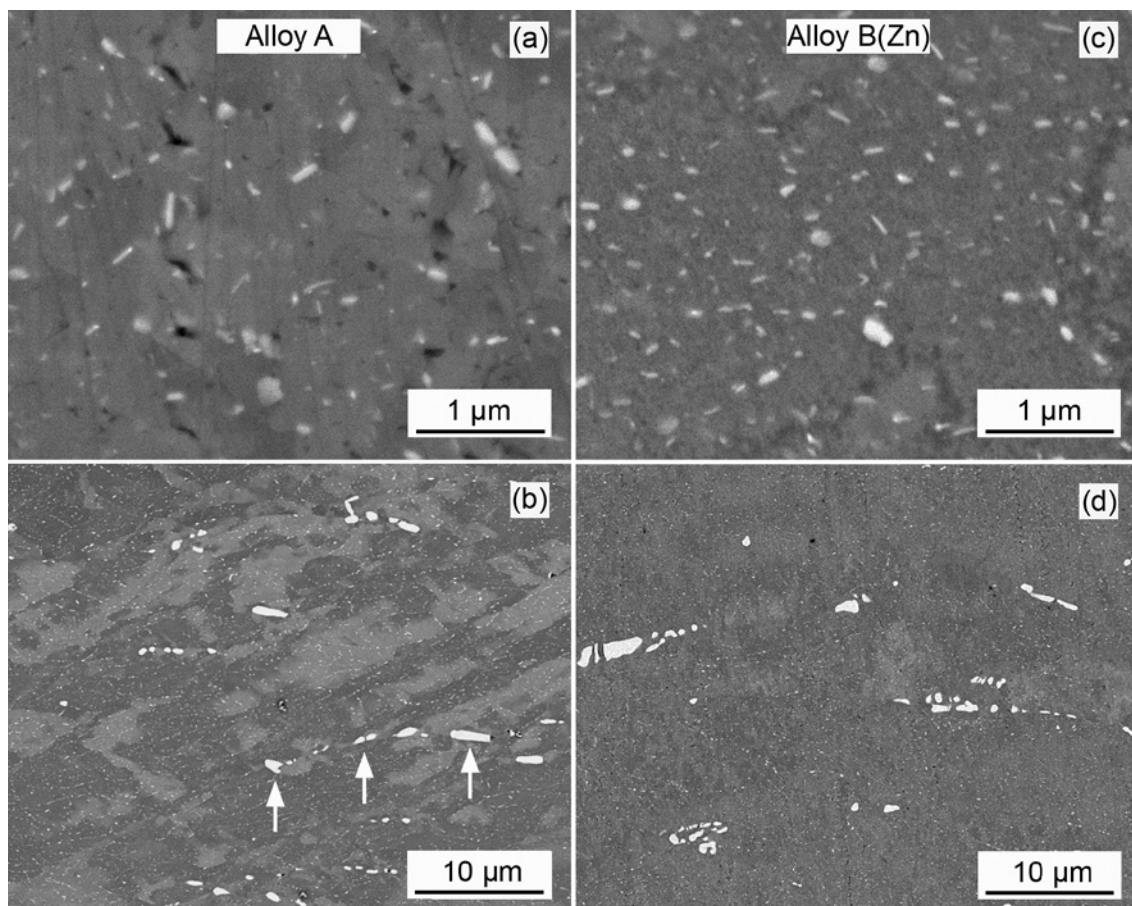


Fig. 5. FEG SEM micrographs of the dispersoids appearing bright in the BSE signal, 5 kV: (a and c) fine particles, (b and d) coarse particles; some of the dispersoid particles are marked by arrows in Fig. 5b, the dark and light grey areas in this micrograph are due to channelling contrast in the grains or subgrains where atomic columns are oriented parallel to the electron beam.

After the whole cycle of the two-step precipitation annealing, quantitative second phase particle analysis on a series of FEG-SEM micrographs was carried out. Figures 5a,c present typical micrographs of fine parti-

cles (magnification  $50\,000\times$ ), and in Figs. 5b,d there are coarse particles recorded at the magnification of  $5\,000\times$ . It can be seen, that in the alloy A, there is apparently lower number density of fine particles

(Fig. 5a) than in the alloy B(Zn) (Fig. 5c), while the coarse particles distribution is practically the same for both alloys. This is also evident from the quantitative phase analysis plotted in Fig. 6. In the alloy B(Zn) there is a higher density of fine particles 20 to 100 nm in size than in the alloy A with low zinc content, the biggest difference (about 60 %) is in the population of the particles having 25 to 35 nm in size (Fig. 6a). The population of coarse particles in both materials is practically the same (Fig. 6b). The reason why Zn has a negligible effect on coarse particles is probably that these particles form from the melt during solidification of the alloy. On the other hand, the fine particles form during precipitation annealing from the solid solution. According to transmission electron microscopy observations on a similar alloy without Zn [20] it follows that during the first step of the precipitation annealing at 250 °C no fine particles form, only clustering of solutes can occur. The nucleation of fine dispersoids (from these clusters) takes place throughout heating from 250 to 450 °C [20]. It is highly probable that higher concentration of atoms in the solid solution (Mn, Si, Cu, Zn) participates in solute clustering and nucleation of small dispersoids. The clusters in the alloy with the addition of 1.66 wt.% of zinc are more frequent, and the number density of nucleated particles is higher than in the alloy without Zn. Sha and Cerezo [23] found Zn in clusters of Al-Zn-Mg-Cu alloy using 3-dimensional atom probe analysis: a positive effect of Zn on the solid solution decomposition was also reported by Guo et al. in an Al-Mg-Si-Cu alloy [24].

#### 4. Conclusions

The effect of zinc addition on the distribution of secondary phase particles in twin-roll cast Al-Mn-Zr alloys was studied. It was found that 1.1 to 1.8 wt.% of zinc enters into constituent Al(Mn,Fe)Si phases; this is practically the same concentration as in the matrix (1.66 wt.%). According to EDXS point analysis, the coarse constituent phases are mainly of the  $\alpha$ -Al<sub>15</sub>(Mn,Fe)<sub>3</sub>Si<sub>2</sub> phase. From the crystallographic point of view, revealed by EBSD, the majority of these particles (> 80 %) are of the cubic variant; the remaining are hexagonal. Quantitative metallographic analysis showed that the addition of zinc improves nucleation of small Al(Mn,Fe)Si particles, 20 to 100 nm in size, which is beneficial for the recrystallization resistance of the alloy. On the other hand, the presence of zinc did not affect the distribution of coarser particles.

#### Acknowledgements

This research has been financially supported by the ERDF in the frame of the project No. CZ.02.1.01/0.0/0.0/

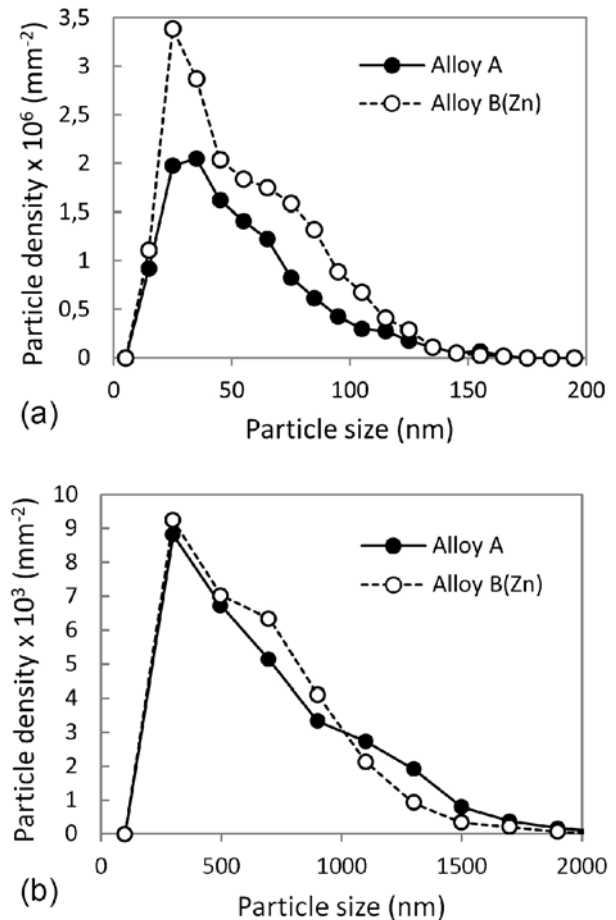


Fig. 6. Distribution of intermetallic particles after the whole cycle of two-step precipitation annealing: (a) fine particles 20 to 200 nm in size, (b) coarse particles 200 to 2000 nm in size.

15\_003/0000485 and of the Czech Science Foundation project 14-36566G. M. V. would like to acknowledge financial support from the Czech Technical University in Prague (project SGS16/249/OHK4/3T/14).

#### References

- [1] Kimura, G., Kawahara, A., Niikura, A., Doko, T., Shinoda, T., Kim, J., Mantis, D.: Furukawa-Sky Review, No. 4, 2008, p. 50. [http://www.uacj.co.jp/review/furukawasky/004/pdf/04\\_abst07.pdf](http://www.uacj.co.jp/review/furukawasky/004/pdf/04_abst07.pdf)
- [2] Humphreys, F. J., Hatherly, M.: Recrystallization and Related Annealing Phenomena. 2nd Edition. Amsterdam, Elsevier 2004.
- [3] Babaghorbani, P., Poole, W. J., Wells, M. A., Parson, N. C.: In: Proceedings of ICAA13. Pittsburgh. Eds.: Weiland, H., Rollett, A. D., Cassada, W. A. Warrendale, The Minerals, Metals & Materials Society 2012, p. 1747.
- [4] Li, Y. J., Muggerud, A. M. F., Olsen, A., Furu, T.: Acta Mater., 60, 2012, p. 1004. [doi:10.1016/j.actamat.2011.11.003](https://doi.org/10.1016/j.actamat.2011.11.003)

- [5] Mondolfo, L. F.: Aluminium Alloys: Structure and Properties. London, Butterworths 1976.
- [6] Cama, H., Worth, J., Evans, P. V., Bosland, A., Brown, J. M.: In: Proceedings of the 4th Decennial International Conference on Solidification Processing. Eds.: Beech, J., Jones, H. Sheffield, University of Sheffield 1997, p. 555.
- [7] Cieslar, M., Slámová, M., Uhlíř, J., Coupeau, C., Bonneville, J.: Kovove Mater., 45, 2007, p. 91.
- [8] Røyset, A., Ryum, N.: Int. Mater. Rev., 50, 2005, p. 19. [doi:10.1179/174328005X14311](https://doi.org/10.1179/174328005X14311)
- [9] Robson, J. D., Prangnell, P. B.: Acta Mater., 49, 2001, p. 599. [doi:10.1016/S1359-6454\(00\)00351-7](https://doi.org/10.1016/S1359-6454(00)00351-7)
- [10] Jia, Z., Hua, G., Forbord, B., Solberg, J. K.: Mater. Sci. Eng. A, 444, 2007, p. 284. [doi:10.1016/j.msea.2006.08.097](https://doi.org/10.1016/j.msea.2006.08.097)
- [11] Jia, Z., Hua, G., Forbord, B., Solberg, J. K.: Mater. Sci. Eng. A, 483–484, 2008, p. 195. [doi:10.1016/j.msea.2006.10.191](https://doi.org/10.1016/j.msea.2006.10.191)
- [12] Hatch, J. E. (Ed.): Aluminum, Properties and Physical Metallurgy. Metals Park, American Society for Metals 1999.
- [13] Jaradeh, M., Carlberg, T.: Metall. Mater. Trans. A, 38, 2007, p. 2138. [doi:10.1007/s11661-007-9251-1](https://doi.org/10.1007/s11661-007-9251-1)
- [14] Güynüz, M., Mollaodlu, A., Ulus, A.: In: Proceedings of Light Metals 2015. TMS Annual Meeting & Exhibition. Ed.: Hyland, M. Berlin, Springer 2016, p. 1255.
- [15] Anselmino, E., Miroux, A., van der Zwaag, S.: Mater. Charact., 52, 2004, p. 289. [doi:10.1016/j.matchar.2004.06.003](https://doi.org/10.1016/j.matchar.2004.06.003)
- [16] Ondráček, J.: Quantitative Analysis of Fine Particles in Al-Mn Alloys. [BSc. Thesis]. Prague, Czech Technical University in Prague, Faculty of Nuclear Sciences and Physical Engineering 2009. (in Czech).
- [17] Qian, M., Taylor, J. A., Yao, J. Y., Couper, M. J., StJohn, D. H.: J. Light Met., 1, 2001, p. 187. [doi:10.1016/S1471-5317\(01\)00012-8](https://doi.org/10.1016/S1471-5317(01)00012-8)
- [18] Gras, Ch., Meredith, M., Hunt, J. D.: J. Mater. Process. Technol., 167, 2005, p. 62. [doi:10.1016/j.jimatprotec.2004.09.084](https://doi.org/10.1016/j.jimatprotec.2004.09.084)
- [19] Belov, N. A., Eskin, D. G., Aksenov, A. A.: Multicomponent Phase Diagrams: Applications for Commercial Aluminum Alloys. 1st Edition. Amsterdam, Elsevier 2005.
- [20] Karlík, M., Vronka, M., Haušild, P., Hájek, M.: Materials and Design, 85, 2015, p. 361. [doi:10.1016/j.matdes.2015.07.023](https://doi.org/10.1016/j.matdes.2015.07.023)
- [21] Li, Y. J., Arnberg, L.: Mater. Sci. Forum, 396–402, 2002, p. 875.
- [22] Poková, M., Zimina, M., Cieslar, M.: In: Proceedings of Light Metals 2015. TMS Annual Meeting & Exhibition. Ed.: Hyland, M. Berlin, Springer 2016, p. 469.
- [23] Sha, G., Cerezo, A.: Acta Mater., 55, 2004, p. 4503. [doi:10.1016/j.actamat.2004.06.025](https://doi.org/10.1016/j.actamat.2004.06.025)
- [24] Guo, M. X., Zhang, Y., Zhang, X. K., Zhang, J. S., Zhuang, L. Z.: Mater. Sci. Eng. A, 669, 2016, p. 20. [doi:10.1016/j.msea.2016.05.060](https://doi.org/10.1016/j.msea.2016.05.060)